Radiative defect state identification in semi-insulating GaAs using photo-carrier Radiometry

2009 Semicond. Sci. Technol. 24 125002

(http://iopscience.iop.org/0268-1242/24/12/125002)

Semicond. Sci. Technol. **24** (2009) 125002 (7pp) doi:10.1088/0268-1242/24/12/125002

Radiative defect state identification in semi-insulating GaAs using photo-carrier Radiometry

Jun Xia and Andreas Mandelis

Department of Mechanical and Industrial Engineering, Center for Advanced Diffusion-Wave Technologies (CADIFT), University of Toronto, Toronto, Ontario M5S3G8, Canada

E-mail: mandelis@mie.utoronto.ca

Received 29 August 2009, in final form 12 October 2009
Published 3 November 2009
Online at stacks.iop.org/SST/24/125002

Abstract

The photo-carrier radiometry (PCR) technique has been applied to a semi-insulating GaAs wafer for the detection and identification of radiative defects. Due to the ultrafast free carrier recombination lifetime, the conventional carrier-diffusion-wave-based PCR theory was modified to reflect the signal domination by trap emission and capture rates in the absence of diffusion. Defect photoluminescence with photon energies from 0.7 to 1.24 eV was collected and analyzed using photo-thermal temperature spectra and resonant (rate-window) detection combined with frequency scans. Five defect levels were identified self-consistently from the combined rate-window and PCR phase data, and the temperature dependence of the defect photoluminescence quantum efficiency was determined through multi-parameter best fits of the PCR rate theory to the experimental data.

Introduction

The defect characterization of semi-insulating (SI) GaAs is of great importance for the performance and optimization of SI-GaAs based optoelectronic and microelectronics devices. In the past few years, significant efforts have been made on the identification of defect states using techniques such as photo-induced current spectroscopy (PITS) [1], piezoelectric photo-thermal (PPT) [2] technique and the newly developed fully non-contacting deep level photo-thermal spectroscopy (DLPTS) [3]. All these approaches are based on a pump-and-probe rate-window detection [4] that measures the post-excitation thermal resonance of current, thermal radiation or optical absorption. Although GaAs is known as an important radiative emission (photoluminescent, PL) material, few PL kinetic/dynamic studies have been reported due to its ultrafast recombination lifetime (within nanoseconds) [5, 6].

In this study, the defect-induced photo-carrier radiometry (PCR) [7] signals from SI-GaAs are analyzed for the first time using photo-thermal emission and capture kinetics, the rate-window technique and laser-beam modulation frequency scans. PCR blocks the non-radiative components by spectral matching of the defector bandwidth to the photon emission spectral range. The conventional PCR theory is based on carrier-diffusion-dominated luminescence emission delay [7]. For SI-GaAs, due to the ultrafast free carrier recombination lifetime, carrier diffusion is negligible. The slow luminescence mainly comes from the thermal relaxation (capture and emission) of defect carriers. Therefore, the diffusion-based PCR model is also modified to reflect this change.

Carrier recombination and photoluminescence in GaAs

Mainly, there are three recombination mechanisms in GaAs, namely, the band-to-band recombination, Shockley-Read-Hall (SRH) recombination, and Auger recombination [8]. Since Auger recombination normally occurs under high carrier concentrations, it is negligible in semi-insulating GaAs. Band-to-band recombination emits photons with bandgap energy ($\sim$1.5 eV) and is blocked by our spectral filter. The SRH recombination is a two-step process that involves (i) trapping of carriers into defect states and (ii) recombination of trapped carriers. Since SRH recombination emits a photon with less than bandgap energy, it is the main contribution to the PCR signal. There are two distinct SRH centers, namely recombination centers and traps. The recombination centers

have similar electron and hole capture coefficients and are the dominant recombination mechanism in GaAs. Traps, however, have a larger capture cross-section for carriers of one sign (electrons or holes) and are more likely to hold and allow carriers of the opposite sign to recombine at a much slower rate [8]. In order to capture carriers of both signs, SRH recombination centers are usually states that lie deep within the energy gap. It should be noticed that, although SRH recombination normally occurs between defects and conduction/valance bands, it may also occur between defect states. Such transitions have been suggested for several PL bands in SI-GaAs [9, 10] and are the main contribution to the slowly decaying luminescence.

The association of defects with PL bands has been investigated in a variety of ways, including (a) examining the photo-quenching (EL2 characteristic) behavior of PL [11], (b) correlation of PL intensity with the distribution of defects [12] and (c) direct identification from the luminescence photon energy [13]. Due to the controlling role of the EL2 level, most PL bands demonstrate an EL2-like behavior [14]. However, there have been several reports suggesting that the EL2 level is not directly related to the PL bands [15]. Several other radiative defects have also been proposed, for instance, the 0.8 eV luminescence band has been variously assigned to (i) an As_{Ga} antisite defect [16], (ii) a V_{Ga} vacancy defect [17], (iii) an As_{Ga}–V_{Ga} complex defect [18] or (iv) the $EL2^{+}$ charge state [14]. Since neither of these studies is based on the thermal kinetics of defect states, they make the direct measurement of activation energy difficult.

Thermoluminescence measurements have also been performed [5, 6]. Due to the ultrafast free-carrier lifetime, the measurement can only be done under limited conditions. For instance, Dao *et al* [5] illuminated the sample with a constant super-bandgap light in order to maintain a high carrier concentration, and Hanna *et al* [6] used a 15 min long integration time to average the weak thermoluminescence signal. All these studies, however, were based on conventional thermoluminescence models, and did not consider recombination between defect states.

To include both recombination involving free carriers and between defect states, an expression is proposed in which the generalized PCR signal is proportional to the density of occupied carriers in the traps, $n_T(t, T)$ (defect recombination), and the free carrier concentration, $n(t)$ (recombination center):

$$L(t, T) = I(T)\left[an(t, T) + b\sum_{j=0}^{l} C_j m_j(t, T) n_{Tj}(t, T)\right]. \tag{1}$$

Here, a and b are constants, $I(T)$ is the un-normalized temperature-dependent emission efficiency for defect j, C_j is the capture cross section; $n_{Tj}(t)$ is the concentration of occupied defect states and $m_j(t)$ is the density of carriers of opposite sign available for recombination with trapped carrier population $n_{Tj}(t)$. In this expression, a constant rate is assumed for recombination involving free carriers. This is a valid assumption in SI-GaAs due to its ultrafast free carrier lifetime [19]. The second term in equation (1) represents recombination between defect states. In these transitions, since activation energies of the two defects are different, one state always holds carriers for a longer period and will simply act as the source of carriers for recombination. For this reason, we can assume $m_j(t)$ to be a constant. This will not affect results of rate-window detection, since only defects with time constants matching (resonant with) the rate-window can be observed. The capture coefficient C_j is the product of thermal velocity v_T and capture cross section σ. Since the carrier thermal velocity is proportional to the square root of temperature [19], C_j obeys the same dependence. Based on the foregoing discussion, equation (1) can be simplified to

$$L(t, T) = I(T)\left[an(t, T) + d\sqrt{T}\sum_{j=0}^{l}\sigma_j n_{Tj}(t, T)\right] \tag{2}$$

where d is a temperature- and time-independent constant.

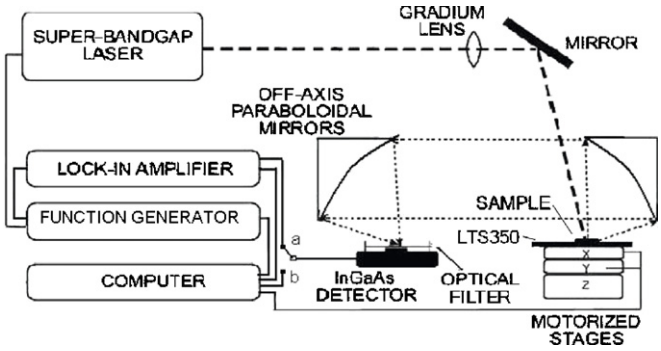

Figure 1. Schematic diagram for photo-carrier radiometry. (*a*) Temperature and frequency scanned modality; (*b*) time-scanned modality.

Experimental setup

The schematic diagram of the PCR experiment is shown in figure 1. The PCR system is a simplified DLPTS system [20] that uses only one super bandgap laser (Melles Griot 56-ICS-270, 830 nm, 100 mW). Detailed description of the system can be found in our previous publications [7, 20]. Several differences should be noticed here. First, the laser is square-wave-modulated instead of a 1% pulse duty cycle (in DLPTS) in order to maintain a high PL intensity. Next, a 1 μm long- pass optical filter is used to block the band-to-band recombination and excitation light. The spectral responsivity of the detector and the filter is shown in figure 2. Therefore, the PCR signal includes carrier radiation emissions from 1 to 1.8 μm wavelength (photon energy 0.7–1.24 eV). Considering the broadening in the luminescence spectra (around 0.35 eV), our PCR signal covers the typical defect luminescence bands (0.67, 0.68, 0.78, 0.8 eV) observed in SI-GaAs [14]. Due to the weak defect luminescence signal, an integration time of 3 s is set in the lock-in amplifier. Samples used in this work are one-side-polished vertical gradient freeze (VGF) grown SI-GaAs wafers with a resistivity of $7.2-7.7\times10^{7}\,\Omega$ cm, etch pit density (EPD) $< 4000\,\mathrm{cm}^{-2}$ and an EL2 concentration around $10^{16}\,\mathrm{cm}^{-3}$ as provided by the vendor.

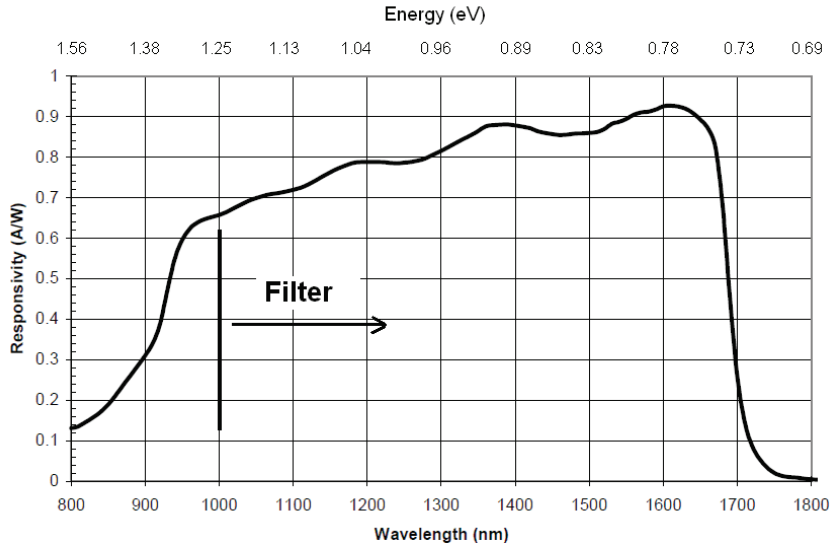

Figure 2. Spectral responsivity of the PCR InGaAs detector. The vertical bold line shows the cutoff wavelength of the longpass filter.

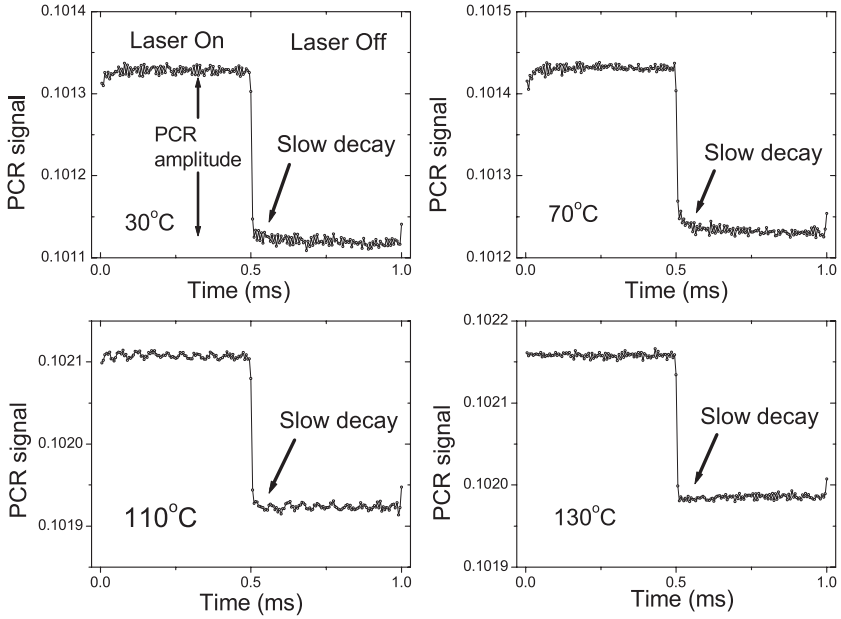

Figure 3. PCR transients from SI-GaAs at various temperatures.

Figure 3 shows PCR transients at various temperatures. At the end of the laser excitation, the signal shows a rapid decrease followed by a slower decay. This slow decay clearly exhibits a decreasing time constant with increasing temperature, which is characteristic of thermal emission from defect states. There is a baseline in the signal that increases with temperature due to black body radiation emission. It should be noticed that, although the PCR technique blocks the thermal radiation from non-radiative carrier recombination, black body radiation still enters the detector. This component, however, is un-modulated and will be blocked by the lock-in amplifier in temperature- and frequency-scanned measurements.

In our DLPTS studies [20], we have demonstrated that the transient signal is the easiest to fit to theoretical models, but it provides the least amount of information about system kinetic parameters. Since the PCR transient is relatively noisier than the temperature- and frequency-scanned spectra due to the lack of lock-in amplifier averaging, our discussion will be mainly focused on spectra instead of transients.

Figure 4 shows the temperature-scanned PCR spectra. The PCR amplitude is only slightly dependent on modulation frequency, and it decreases rapidly when temperature increases. This is so because of the competing non-radiative recombination process which is more probable at high temperatures [21]. The PL efficiency $I(T)/I_0$ (I_0 is the normalizing factor) can be approximated by

$$I(T)/I_0 = \frac{P_r}{P_r + P_{nr}} \tag{3}$$

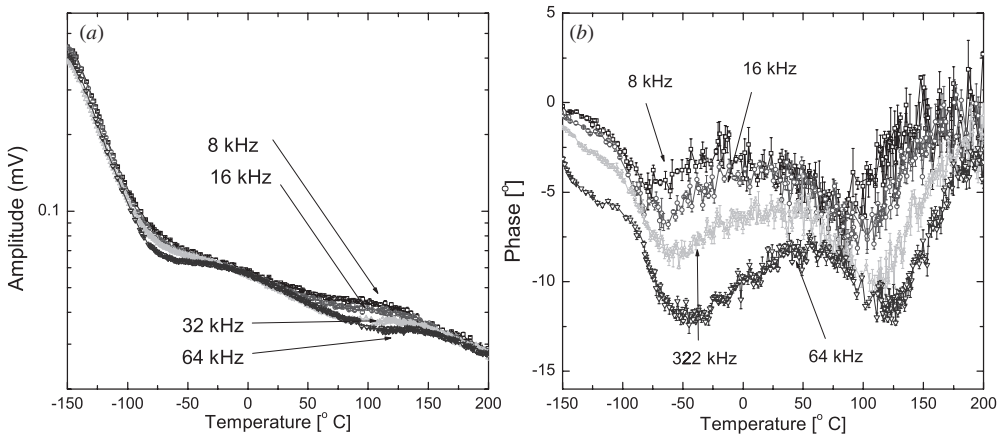

Figure 4. The temperature-scanned PCR spectra at various frequencies. (*a*) Amplitude and (*b*) phase spectra.

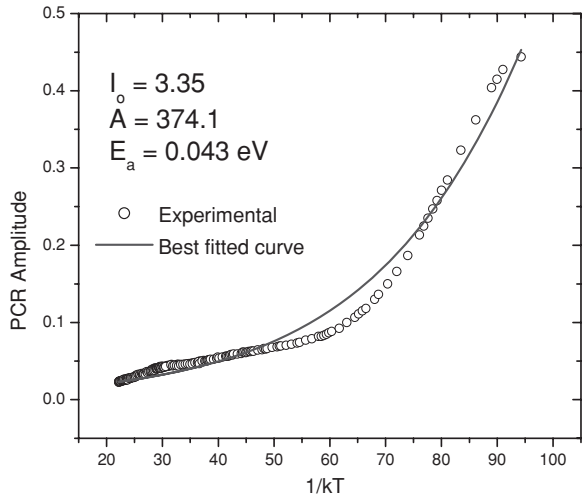

Figure 5. Best-fit of the PL efficiency to the 8 kHz amplitude spectrum to equation (5).

where P_{r} and P_{nr} represent the probability for radiative and non-radiative transitions, respectively. It is normally assumed that P_{r} is a constant, and P_{nr} can be thermally activated

$$P_{\mathrm{nr}}(T) = P_{\mathrm{nr0}} \exp(-E_a/kT). \tag{4}$$

Here E_a is the activation energy for non-radiative recombination. Substituting equation (4) into equation (3), we obtain

$$I(T)/I_0 = 1/[1 + A \exp(-E_a/kT)]. \tag{5}$$

Here $A \equiv P_{\mathrm{nr0}}/P_{\mathrm{r}}$ is a constant. Using equation (5), the 8 kHz amplitude spectrum is best fitted as shown in figure 5. Discrepancies between theoretical and experimental curves are mainly due to the simplifications in equation (5), such as the temperature-independent radiative recombination probability [21], and the absence of defect thermal emission/capture processes. Since carrier emission and capture at defects will greatly affect the radiative recombination within the energy states, a more precise determination of emission efficiency can only be achieved when the defect states have been identified.

The phase spectra (figure 4(*b*)) provide a convenient way to analyze data with unknown $I(T)$. Contrary to amplitude, the phase shows little change as a function of temperature. This is due to the fact that phase represents the ratio of quadrature to in-phase signals, thereby eliminating the $I(T)$ dependence. There are two reversed peaks in the phase spectra, and the peak position shifts to higher temperatures as frequency increases. This further confirms the influence of defect thermal emission in the radiative recombination process. In order to obtain an Arrhenius plot from these reversed peaks, one usually needs to know the ratio between the emission rate at peak temperature and the modulation frequency [19]. This ratio is usually obtained numerically from $n(t)$ (current-based DLTS [1]) or from $n_T(t)$ (capacitance-based DLTS [4]) exclusive models [19]. For our PCR theory (equation (2)) with combined and unknown contributions from $n(t)$ and $n_T(t)$, it is difficult to determine this ratio. Moreover, broadening effects and the resulting defect energy overlaps will further add complexity to direct peak identification [20]. For these reasons, a direct fit to the experimental spectra is used in our study.

Since we had found in our DLPTS studies that the combined time-, frequency- and temperature-scan analysis provides an important (and otherwise unavailable) consistency and fidelity in the identification of defect states [20], frequency scans were also performed as shown in figure 6. For clarity, the amplitude scans are normalized with respect to the maximum amplitude at each temperature, and both amplitude and phase scans are intentionally separated by amounts shown next to each curve temperature in the figure inset. It can be seen that amplitudes decrease and phase lags increase with increasing frequency, a clear indication of the existence of slow photo-thermal kinetics consistent with long thermal emission times in SI-GaAs.

To avoid dealing with the unknown luminescence efficiency $I(T)$, theoretical best-fits were applied only to the temperature phase spectra and to the amplitude and phase frequency scans, but not to the temperature amplitude spectra. A hybridized Genetic and Nelder–Mead algorithm [22] was used for multi-parameter fitting. This hybridized approach combines the advantage of global (Genetic) and local (Nelder–Mead) search and is more efficient in finding the global minima of the object function (difference between the experimental and theoretical model data).

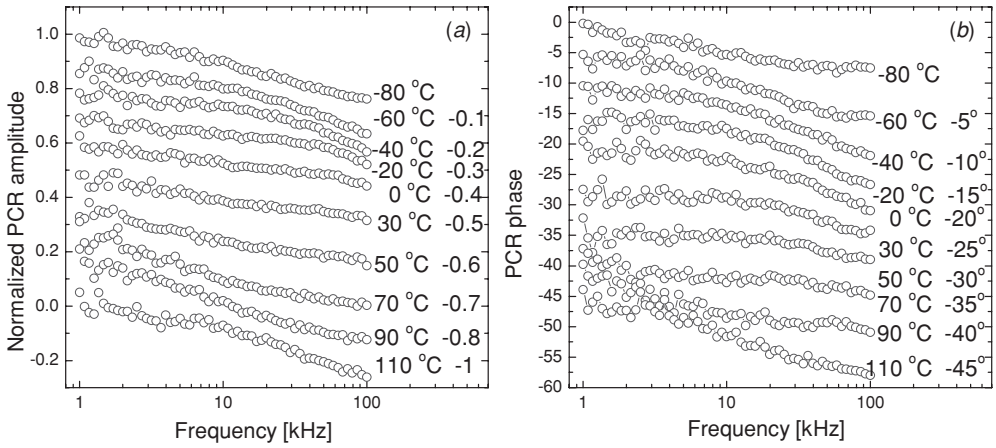

Figure 6. Frequency-scanned PCR signals at various temperatures. (*a*) Amplitude and (*b*) phase. The curves at all temperatures have been shifted downward for clarity by amounts indicated in the inset.

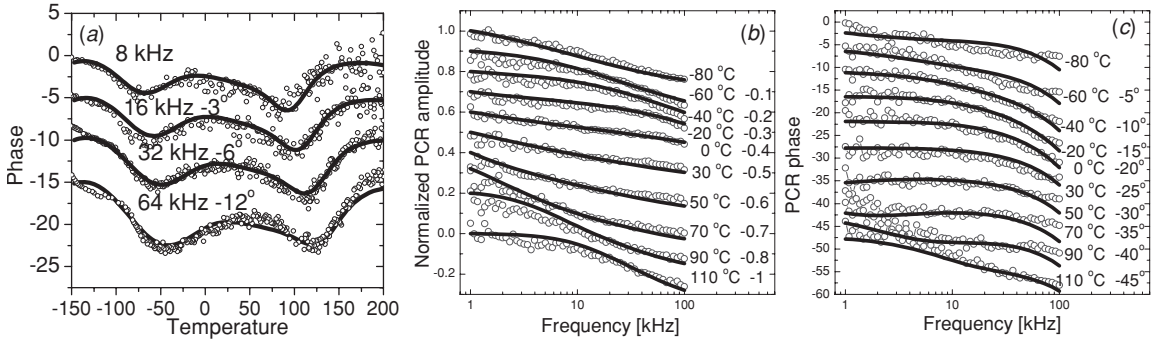

Figure 7. Experimental and theoretical PCR data: (*a*) temperature-scanned phases; (*b*) frequency-scanned amplitudes; (*c*) frequency-scanned phases.

In the best-fit procedure, the simplified DLPTS model with stretched exponential broadening was used [20, 23]. For $t \leqslant t_p$ (t_p: laser pulse width)

$$n(t) = G^{\mathrm{op}}\tau_n(1 - \mathrm{e}^{-t/\tau_n}), \tag{6}$$

$$n_T(t,T) \equiv \sum_{j=0}^{m} n_{Tj}(t,T) = \sum_{i=0}^{m} \frac{N_{Tj}}{1 + (e_{nj}/G^{\mathrm{op}}\tau_n C_{nj})} \times [1 - \mathrm{e}^{-(G^{\mathrm{op}}\tau C_{nj} + e_{nj})t}]. \tag{7}$$

For $t > t_p$

$$n(t,T) = \sum_{j=1}^{m} \frac{e_{nj}}{\tau^{-1} - e_{nj}} n_{Tj}(t_p)\left[\mathrm{e}^{-((t-t_p)e_{\mathrm{nj}})^{\beta_{\mathrm{j}}}} - \mathrm{e}^{-(t-t_p)/\tau_n}\right] + n(t_p)\,\mathrm{e}^{-(t-t_{\mathrm{p}})/\tau_{\mathrm{n}}}, \tag{8}$$

$$n_{Tj}(t,T) = n_{Tj}(t_p,T)\exp\{-[e_{nj}(t-t_P)]^{\beta_j}\}. \tag{9}$$

Here $G^{\mathrm{op}}(t)$ is the optical generation rate, τ_n is the free carrier recombination lifetime. For a defect level j, E_j is the activation energy, C_{nj} is the capture coefficient. N_{Tj} is the defect or trap concentration and $e_{nj}(E_j)$ is the thermal emission rate. It can be seen that, during the pulse, defect states are filled at a rate of $(G^{\mathrm{op}}\tau C_{nj} + e_{nj})$, and after the end of the pulse, defect states thermally emit carriers at rate $e_{nj}(E_j)$. $\beta(T) = 1/[1 + \Delta E_0/(k_B T)]$ represents the hierarchical carrier emission-induced spectrum broadening [20].

The best-fitting procedure starts with two defect levels, and then gradually adds more defects until a good fit is obtained. Since the initial condition for the Genetic algorithm is randomly generated, the convergence of the best-fit results was verified by running the program several times. The solid lines in figure 7 show the best-fitted spectra. Five defects were identified and summarized in table 1. Similar to DLPTS, the defect concentration N_T needs to be corrected once parameters a and d in equation (2) are determined. In our theoretical simulation, the values of 3 and 1×10^{-2} were used, based, respectively, on the approximate contribution of $n(t)$ and $n_T(t)$ to the 70 °C transient. From the PCR model in equations (2) and (6)–(9), it can be seen that different a and d values affect the value of N_T only.

The first two defects shown in table 1 could both be the EL2 level considering the fact that EL2 consists of several charge states with different activation energies ranging from 0.85 to 0.6 eV [24, 25]. Since our calculation is based on defect-to-defect recombination, this PCR result supports the Kaminska and Weber's model [25], i.e. that the 0.67 eV PL is a result of intra-center transitions within EL2. The EL4 defect is known to be a Ga vacancy defect, which has been suggested for the observed 0.8 eV PL band [14]. The defect level at 0.2 eV could either be the EL17 or EL14 level [26, 27].

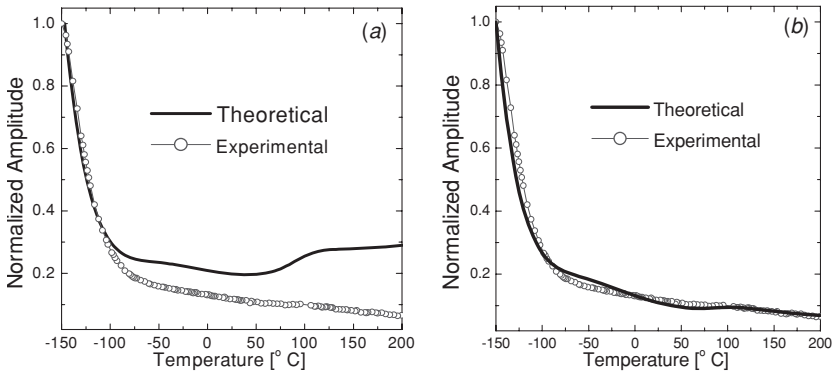

Figure 8. Experimental and theoretical PCR temperature-scanned spectra at 8 kHz modulation frequency: (*a*) without, and (*b*) with luminescence efficiency temperature dependence.

Table 1. Summary of defect states detected by PCR.

	E_n (eV)	σ ($\times 10^{-13}$ cm^2)	N_T ($\times 10^{15}$ cm^{-3})	ΔE (eV)
EL2	0.87	0.0131	0.3275	0.0151
EL2	0.69	36.9581	0.0326	0.002
EL4	0.52	4.1017	0.0356	0.0585
EL14	0.2	0.0053	0.0521	0.0166
Shallow donor	0.066	0.0623	1.7707	0.0374

Since EL14 is known to be a Ga and As complex vacancy defect, which is consistent with Lagowski's [17] model for 0.82 eV luminescence, we tentatively identified the 0.2 eV defect to be the EL14 level. A shallow defect state was also found. This could be the shallow donor defect proposed by Yu [9] responsible for the 0.77 eV radiative transition. The consistency of our results with previous dc PL studies and the ability to extract self-consistent defect parameters as a result of three signal-generation processes (time, frequency, and temperature scans) further demonstrate the defect diagnostic power of the PCR technique. Compared with DLPTS, PCR detects fewer defect levels (5 versus 11) due to its radiative detection mechanism. Non-radiative defects are not monitored in PCR, while they can still be seen in DLPTS by use of the probe beam. However, PCR identifies two charge states of the EL2 level and a shallower defect level, which are not observed in the DLPTS results. So PCR and DLPTS are complementary to each other, and combining the two techniques enables a more comprehensive characterization of SI-GaAs. Similar to DLPTS, the defect concentration N_T needs to be corrected once the actual luminescence efficiency (b in equation (1), d in equation (2)) is known. The same holds for the capture cross section σ which also needs to be corrected as shown in equation (2). However, these corrections will not affect the application of our PCR technique since the activation energy is the most important and sensitive parameter of defect states, while both capture cross section and defect concentration may vary from technique to technique due to different detection mechanisms [18, 27].

With the identified defects, the 8 kHz PCR temperature-scanned amplitude spectra were best fitted to theory as shown in figure 8(*a*). In this simulation, the PL efficiency $I(T)/I_0$ was assumed to be a constant. It can be seen that even with a temperature-independent I/I_0, the simulated spectra exhibit decaying curve versus temperature. Discrepancies start to appear near -100 °C. This is consistent with observations in thermoluminescence measurements that the luminescence efficiency remains constant up to a critical temperature and then decreases rapidly [28]. This also supports our argument that $I(T)$ is affected by the thermal emission process from defect states. By using best-fitted theoretical simulations in the temperature spectra shown in figure 7(*a*), the temperature-dependent PL efficiency, $I(T)/I_0$, can be derived giving $I_0 = 5.97$, $E_a = 0.1$ eV and $A = 34.9$ in equation (5). Figure 8(*b*) shows the theoretical spectra using $I(T)/I_0$. It can be seen that the fit is greatly improved. However, small discrepancies still exist. This could be due to the fact that the same PL efficiency is used for all defect states, while it is possible that each defect has its own efficiency. Using a different $I(T)$ for each defect, however, will increase uncertainties in the fitting parameters and can only be achieved when some of the defect parameters are pre-known. The good agreement between the experiment and our theory for both temperature and frequency scans proves that our modified and simplified rate-dependent but not diffusion-dependent PCR model is well suited for the detection of radiative defects in SI-GaAs.

Conclusions

The PCR technique has been applied to SI-GaAs for the study of defect PL as a result of carrier emission photo-thermal processes. The temperature-scanned phase spectra and the frequency scans provide a convenient way to analyze the data without using the temperature-dependent PL efficiency, which can be determined independently once the defect states are identified. Five defect states were identified through a multiparameter fitting method of the PCR capture- and emission-rate theory applied to the experimental data.

The calculated energy levels are consistent with studies of conventional dc PL measurements. However, compared with dc PL measurements, our modulated rate-window photothermal methodology for probing radiative recombination transitions is extremely sensitive to defect activation energies and low concentrations, which makes the identification of radiative defects much easier. In addition, the combined self-consistent study in several domains (transient, frequency-scan and photo-thermal temperature-scan) makes the multi-defect-parameter fitting possible and multiple defect assignments unique. This combined analysis provides additional accuracy and consistency in the identification of highly overlapped defect states, which are indistinguishable in single domain studies. Based on the results of this study, our PCR technique has great potential to be developed as a fully noncontact characterization tool for radiative defect state studies in semiconductor materials.

Acknowledgments

The authors are grateful to the Natural Sciences and Engineering Research Council of Canada (NSERC) for its support for this project through a Discovery Grant to A.M. They also gratefully acknowledge the support of the Canada Research Chairs program and the Ontario Premier's Discovery Inaugural (2007) Award. Valuable discussions with Dr Anna Matvienko in the Simplex program are also acknowledged.

References

[1] Hurtes C, Boulou M, Mitonneau A and Bois D 1978 *Appl. Phys. Lett.* **32** 821
[2] Fukuyama A, Memon A, Sakai K, Akashi Y and Ikari T 2001 *J. Appl. Phys.* **89** 1751
[3] Xia J and Mandelis A 2007 *Appl. Phys. Lett.* **90** 062119
[4] Lang D V 1974 *J. Appl. Phys.* **45** 3023
[5] Dao L V, Kraft E, Gal M, Fu L and C Jagadish 2000 *Semiconducting and Insulating Materials Conf., 2000. SIMC-XI. International* p 141
[6] Hanna S and Seilmeier A 2006 *Solid State Commun.* **137** 557
[7] Mandelis A, Batista J and Shaughnessy D 2003 *Phys. Rev.* B **67** 205208
[8] McKelvey J P 1966 *Solid State and Semiconductor Physics* (New York: Harper and Row)) chapter 10
[9] Yu P W 1984 *Phys. Rev.* B **29** 2283
[10] Bourgoin J C, von Bardeleben H J and Stievenard D 1988 *J. Appl. Phys.* **64** R65
[11] Tajima M 1987 *Japan. J. Appl. Phys.* **226** L885
[12] Hovel H J and Guidotti D 1985 *IEEE Trans. Electron Devices* **32** 2331
[13] Yu P W, Robinson G D, Sizelove J R and Stutz C E 1994 *Phys. Rev.* B **49** 4689
[14] Hamilton B 1996 *Properties of Gallium Arsenide* ed M R Brozel and G E Stillman (London: INSPEC)) chapter 9
[15] Samuelson L, Omling P and Grimmeiss H G 1984 *Appl. Phys. Lett.* **45** 521
[16] Windscheif J, Ennen H, Kaufmann U, Schneider J and Kimura T 1983 *Appl. Phys.* A **30** 47
[17] Lagowski J, Gatos H C, Parsey J M, Wada K, Kaminska M and Walukiewicz W 1982 *Appl. Phys. Lett.* **40** 342
[18] Shinohara M 1987 *J. Appl. Phys.* **61** 365
[19] Look D C 1983 *Semiconductors and Semimetals* vol 19 ed R K Willardson and A C Beer (New York: Academic) p 75
[20] Xia J and Mandelis A 2009 *J. Appl. Phys.* **105** 103712
[21] Pankove J I 1971 *Optical Processes in Semiconductors* (Englewood Cliffs, NJ: Prentice-Hall)) chapter 6,7
[22] Chelouah R and Siarry P 2003 *Eur. J. Oper. Res.* **148** 335
[23] Mandelis A and Xia J 2008 *J. Appl. Phys.* **103** 043704
[24] Bourgoin J C and Neffati T 1999 *Solid-State Electron.* **43** 153
[25] Kaminska M and Weber E R 1993 *Imperfections in III/V Materials* vol 38 (San Diego, CA: Academic) p 59
[26] Kaminski P and Kozlowski R 2002 *Mater. Sci. Eng.* B **91–92** 398
[27] Martin G M, Mitonneau A and Mircea A 1977 *Electron. Lett.* **13** 191
[28] McKeever S W S 1985 *Thermoluminescence of Solids* (Cambridge: Cambridge University Press) chapter 2